Journal of Intelligent & Robotic Systems (2023) 109:80
https://doi.org/10.1007/s10846-023-02013-y

REGULAR PAPER

Human–Robot Collaborative Lifting Motion Prediction and Experimental Validation

Asif Arefeen[1] · Joel Quarnstrom[1] · Shahbaz P. Qadri Syed[1] · He Bai[1] · Yujiang Xiang[1]

Received: 24 August 2022 / Accepted: 2 November 2023

Abstract
This paper presents a human–robot collaborative symmetric lifting motion prediction using inverse dynamics optimization. The human and robot arm are modeled in Denavit-Hartenberg (DH) representation. A floating-base rigid body with 6 global degrees of freedom (DOFs) is similarly modeled as a three-dimensional (3D) table. A set of grasping forces characterizes the human-table and robot-table interactions. The joint torque squares of human arm and robot arm are minimized and subjected to physical and task related constraints. During lifting, the design variables include the cubic B-spline control points of joint angle profiles of the human arm, robot arm, and table. In addition, the discretized grasping forces are also treated as design variables. Both numeric and experimental human–robot lifting was performed with a 2 kg table. The simulation reports the human and robot arm's joint angle profiles, joint torque profiles, and grasping force profiles. These profiles were validated with experimental data, which was collected using a motion capture system, force sensors, and the robot operating system (ROS). The human and robot arms' joint angle and torque profiles demonstrate a similar trend in the experimental environment. The grasping force comparison implies that the human and robot share the load while lifting together.

Keywords Motion planning · Human–robot lifting · Motion capture · Force sensors · ROS · Inverse dynamics optimization · and optimization

1 Introduction

Human–robot interaction is a topic of study with numerous applications and a significant impact on the economy [1]. Collaboration between humans and robots can significantly accelerate production processes, enhance manufacturing quality, and lower structural costs [2]. However, it is necessary to predict the human–robot lifting motion with grasping forces to avoid human injuries. Researchers have developed various biomechanical prediction models for lifting over the previous few decades [3–7]. Furthermore, human–robot interaction research has made significant progress. This paper aims to use optimization techniques to design, simulate, and validate a human–robot collaborative symmetric optimal lifting motion.

Researchers are currently using different learning techniques to successfully anticipate and execute lifting tasks. Evrard et al. [8] presented a controller which learned from a demonstration and was used to conduct a human–robot collaborative task with the help of a human operator. After learning, the robot could do collaborative lifting by conditioning the Gaussian Mixture Model (GMM) with the perceived force/torque. It generated the velocity response using Gaussian Mixture Regression (GMR). By adjusting the impedance controller parameters, Evrard and Kheddar [9] were able to allocate leader/follower roles and solve the challenge of determining the robot's involvement in a collaborative lifting operation. Furthermore, DelPreto and Rus [10] used electromyography (EMG) signals to estimate the human's intention in a real-time interface for controlling collaborative lifting tasks. Calinon et al. [11] studied a robotic learning system to reproduce collaborative lifting with a haptic interface. The probabilistic relationships between the forces and the task's kinematic characteristics were continually encoded. Then the robot was able to choose a controller on its own to replicate the collaboration skill with the desired behavior. Agravante et al. [12] proposed an integrated framework that utilizes a visual servoing controller to perceive the task and a haptic channel to detect human intent. The

✉ Yujiang Xiang
yujiang.xiang@okstate.edu

[1] School of Mechanical and Aerospace Engineering, Oklahoma State University, Stillwater, OK 74078, USA

Published online: 24 November 2023

impedance control framework combined vision and force control, affecting all degrees of freedom (DOFs) simultaneously. Collaboratively lifting a table while keeping a ball on it is the job that was completed. In a collaborative task, Lawitzky et al. [13] proposed a novel approach that combined planning and learning-based approaches. The recorded force readings were used by the robot to follow human supervision throughout the initial learning phase. Using measured force and motion data to train a Hidden Markov Model (HMM) to anticipate the human's subsequent actions, the robot gradually learned to take a more active role. Sheng et al. [14] presented an integrated human–robot collaborative framework that utilizes imitation and reinforcement learning to make a table stay horizontally between the human and robot. A reactive controller attempted to keep the system stable, while proactive actions were taken by a proactive controller based on human motion prediction. Both holding the table steady and controlling the table were taught through imitation learning. The findings reveal that confidence in the motion predictor was used to switch controller modes automatically, and that this method works well for collaborative manipulation. A model for human–robot haptic collaboration was proposed by Rozo et al. [15]. Their technique learned to map reported forces to the impedance parameters required to actuate the robot through the demonstration. In [16], the author applied a task-parameterized GMM-based technique for cooperative transportation tasks, which allows for structuring the robot's mobility as a function of the task parameters and optimal control. It was extended by adding stiffness estimates based on a convex optimization in [2]. Wang et al. [17] designed a robot controller that uses an HMM-based high-level controller to encode motion trajectories. It was used to predict human intentions and adjust the reference trajectory as needed based on haptic input of the current human state at each time point.

On the other hand, force/torque sensors and optimization techniques have been used for intention prediction and optimal motion prediction by several researchers. A cooperative manipulation task was presented in [18], in which a human and a robot worked together to move a large table. Force/torque sensors were used to identify the intent, and a mathematical model was utilized to process their findings. Task modeling produced a role allocation parameter which enabled leader–follower role arbitration. The user was given a haptic input via the cooperatively manipulated object. A 1 DOF impedance control law proposed by Bussy et al. [19] created a time-dependent reference trajectory path for a robot to follow in order to achieve the required trajectory. The robot anticipates the human's intended movement by identifying a collection of primitive motions and constructs a time-dependent trajectory consistent with the prediction in a combined table-carrying task. The process was repeated with the robot being teleoperated by another person, and in this case, the human lifter followed the robot's lead. Furthermore, to adjust the robot's behavior, wrist-mounted force-torque sensors were added to the robot. Li et al. [20] calculated target positions using force. As the robot plays a more proactive role, estimating the human's desired target position reduces the amount of power the robot should exert. An impedance controller was used to incorporate the human's predicted motion. Passenberg et al. [21] utilized a 2-DOF haptic device to simulate a human–robot interaction. The interaction forces were used to accomplish the autonomous response. They determined the optimal assistance levels for specific tasks based on a human's effort and task performance criteria. In [22], a dynamical human model was developed that uses a Lagrangian formulation to describe the relationship between contact points and the resulting contact force. The statically equivalent serial chain approach was used for the human model structure. During a co-manipulation or handover task, the human's pose was optimized to minimize torque on the human joints. In terms of the Rapid Entire Body Assessment (REBA) score, Van der Spaa et al. [23] optimized a discrete sequential plan of postures for human–robot cooperation tasks. It was also noted that it was too computationally expensive to be used for online planning. Xiang et al. [6] developed a human–human collaborative lifting motion prediction with grasping forces. In addition, an optimization-based human–robot collaborative lifting motion prediction was developed in previous research [24].

A few research focuses on human–robot cooperation for precise object positioning and human adaptability. Wojtara et al. [25] constructed a robotic system to place an object on a surface with precision. The human interacts with the robot's impedance to adapt to the final position, whereas the robotic system just has a general location of the goal position. Maurice et al. [26] presented a study on the human's ability to adapt to non-biological movements when the human and the robot lift together. It was reported that a robot that moved along a course in a biological velocity pattern rather than a predetermined velocity pattern helped the human function better, and the human exerted less force on the robot. Parker and Croft [27] studied human following behavior in a cooperative vertical object lifting task as a response to a leading robotic manipulator. They discovered that the pace of the task and differences across subjects had a substantial impact on the results.

The proposed work uses inverse dynamics optimization to predict the human–robot collaborative symmetric lifting motion and the grasping forces. A sequential quadratic programming (SQP) algorithm in a sparse nonlinear optimizer (SNOPT) [28] is used to solve the human–robot lifting problem. The predicted optimal results are used in the experimental human–robot lifting setup. Valid comparisons are established between the simulation and experiment. Therefore, the predicted optimal human–robot lifting motion and grasping forces can mitigate human injuries during

human–robot interaction. Table 1 summarizes the state-of-the-art methods for human–robot collaborative lifting.

The proposed optimization based method has several advantages: 1) we formulate a computationally efficient optimization model for human–robot collaborative lifting; 2) the simulation can generate the optimal trajectories for the human–robot lifting; 3) the optimization formulation can optimize the grasping forces between human and table, and robot and table 4) we propose an easy and practical method to measure the grasping forces in real time in experiment. The major limitation for the current model is that the robot motion is pre-simulated and is not able to response to human adaptations during the lifting process. Learning-based methods can overcome this limitation, but they require numerous demonstrations and complicated training procedures. In this study, we focus on proposing a novel optimization formulation to predict collaborative human–robot lifting motion, optimize the grasping forces, and validate the simulation with experiments.

The contents of this article are organized as follows: the human–robot modeling method is first described in Section 2, and the equations of motion (EOM) and sensitivities are also detailed. Section 3 covers the details of the experimental method. The optimization formulation for the human–robot lifting problem is presented in Section 4. Section 5 presents simulation conditions, results, and

Table 1 Comparisons of the human–robot lifting methods in the literature

Reference	Human model	Robot	Interaction information	Simulation method
Evrard et al. [8]	Human subject	30-DOF HRP (Humanoid Robotics Project)-2 humanoid robot	Haptic interaction	Gaussian Mixture Model (GMM) and Gaussian Mixture Regression (GMR) learning algorithms
DelPreto and Rus [10]	Human subject	7-DOF Rethink Baxter robot (one arm)	Human muscle activity via EMG	Experimental and genetic algorithm for parameters optimization
Lawitzky et al. [13]	Human subject	7-DOF mobile robot	Contact forces and motion data	Feedback planning and learning based motion prediction approaches
Sheng et al. [14]	Human subject	25-DOF Nao humanoid robot	Human–robot relative position	Reinforcement learning
Bussy et al. [19]	Human subject	30-DOF HRP-2 (Humanoid Research Project-2)	A collection of human primitive motions	Compliant position control method
Peternel et al. [22]	5-DOF 2D model	7-DOF Kuka Lightweight robot arm	Experimentally measured contact forces and muscle activity	Constrained optimization
Van der Spaa et al. [23]	Human subject	32-DOF bimanual mobile robot	Human's pose and external forces	Experimental data-based supervised learning and graph search algorithm
Parker and Croft [27]	Human subject	6-DOF CRS (Cylindrical Revolute Spherical) A460 articulated robot arm	Vertical displacement of object ends	Experimental approach
Lorenzini et al. [29]	Human subject	7-DOF Kuka Lightweight robot arm	Human's pose and visual feedback	Feed-forward artificial neural network (ANN)
Roveda et al. [30]	Human subject	7-DOF Kuka iiwa (intelligent industrial work assistant) 14 R820	Muscle activity and vision	ANN
Kim et al. [31]	5-DOF human model	7-DOF Kuka Lightweight robot arm	Experimentally measured human's pose, vertical ground reaction forces (GRF) and interaction forces	Constrained optimization
Sartore et al. [32]	48- DOF human model	53-DOF iCub humanoid robot	Robot energy expenditure	Interior point method for nonlinear optimization
Al-Yacoub et al. [33]	Human subject	15-DOF SDA (Slim Dual Arm) 10D dual-arm robot	Haptic interaction	Random forest (RF) and weighted random forest (WRF) regression methods
Arefeen et al. [34]	13-DOF 3D arm	10-DOF Sawyer robot arm	Table location and optimized grasping forces	Gradient-based optimization

experimental validations. Finally, discussion and concluding remarks are given in Section 6.

2 Human–robot Model and Equation of Motion

The recursive Lagrange approach is used in this section to describe the human–robot modeling and EOM for the human–robot and table systems.

2.1 Human–robot System

This study takes into account a 13-DOF 3D human skeleton arm model and a 10-DOF robot arm model. A floating-base rigid table with 6 DOFs is also utilized for lifting, as illustrated in Fig. 1. The skeletal arm model and robot arm model consist of one physical arm branch and one virtual branch, including the global DOFs. The human skeletal arm branch includes the upper spine, shoulder, elbow, and wrist joints. In this work, we only considered the arm lifting of a lightweight table collaboratively with a robot, and the whole-body waist joint was not considered. The Denavit-Hartenberg (DH) approach was used to construct all models [35]. Furthermore, two grasping force vectors (f_1^c and f_2^c) act on the table's two bottom edges. In this study, human anthropometric data are generated from generator of body data (GEBOD) [36].

The DH parameters for the human, robot, and table models are described in Tables 2, 3, and 4, respectively. The required link lengths and mass data of the robot arm model are available in the literature [37]. A revolute joint has variable (motion) on θ, and a prismatic joint has variable on d. The default DH parameters define the original configuration, DOFs' sequence, and the local coordinates' orientations. When we apply the DH parameters to the transformation matrices, the motion variables (x_θ for a revolute joint and x_d for a prismatic joint) should add the default corresponding DH parameters for the human, robot, and table.

Table 2 DH parameters for human arm model

DOF	$\boldsymbol{\theta}$ (rad)	$\boldsymbol{d}$ (m)	$\boldsymbol{a}$ (m)	$\boldsymbol{\alpha}$ (rad)	Translation/ Rotation
1	$\pi/2$	0	0	$\pi/2$	Global translation (GT1)
2	$\pi/2$	0	0	$\pi/2$	Global translation (GT2)
3	$\pi/2$	L_1	0	$\pi/2$	Global translation (GT3)
4	$\pi/2$	0	0	$\pi/2$	Joint rotation (Q1)
5	$\pi/2$	0	0	$\pi/2$	Joint rotation (Q2)
6	$-\pi/2$	L_2	L_3	$-\pi/2$	Joint rotation (Q3)
7	$\pi/2$	0	0	$\pi/2$	Joint rotation (Q4)
8	$-\pi/2$	0	0	$\pi/2$	Joint rotation (Q5)
9	0	$-L_4$	0	$\pi/2$	Joint rotation (Q6)
10	0	0	0	$\pi/2$	Joint rotation (Q7)
11	0	L_5	0	$-\pi/2$	Joint rotation (Q8)
12	$\pi/2$	0	0	$-\pi/2$	Joint rotation (Q9)
13	0	0	$-L_6$	0	Joint rotation (Q10)

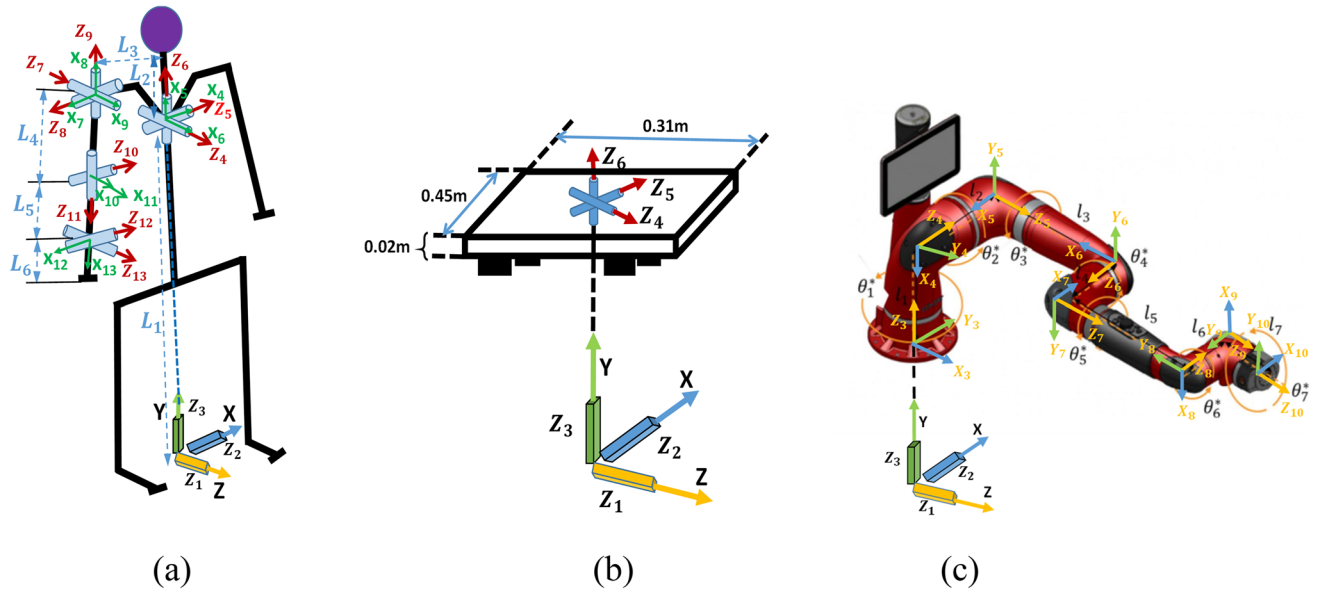

Fig. 1 **a** The 3D human skeletal arm model, **b** 3D table model, and **c** Sawyer robot arm

Table 3 DH parameters for robot arm model

DOF	$\boldsymbol{\theta}$ (rad)	$\boldsymbol{d}$ (m)	$\boldsymbol{a}$ (m)	$\boldsymbol{\alpha}$ (rad)	Translation/ Rotation
1	$\pi/2$	0	0	$\pi/2$	Global translation (GT1)
2	$\pi/2$	0	0	$\pi/2$	Global translation (GT2)
3	0	l_9	0	0	Global translation (GT3)
4	0	l_1	l_2	$-\pi/2$	Joint rotation (Q1)
5	$-\pi/2$	l_3	0	$-\pi/2$	Joint rotation (Q2)
6	π	l_4	0	$\pi/2$	Joint rotation (Q3)
7	0	l_5	0	$-\pi/2$	Joint rotation (Q4)
8	0	l_6	0	$-\pi/2$	Joint rotation (Q5)
9	π	l_7	0	$-\pi/2$	Joint rotation (Q6)
10	$-\pi/2$	l_8	0	0	Joint rotation (Q7)

Table 4 DH parameters for table model

DOF	$\boldsymbol{\theta}$ (rad)	$\boldsymbol{d}$ (m)	$\boldsymbol{a}$ (m)	$\boldsymbol{\alpha}$ (rad)	Translation/ Rotation
1	$\pi/2$	0	0	$\pi/2$	Global translation (GT1)
2	$\pi/2$	0	0	$\pi/2$	Global translation (GT2)
3	$\pi/2$	0	0	$\pi/2$	Global translation (GT3)
4	$\pi/2$	0	0	$\pi/2$	Global rotation (GR1)
5	$\pi/2$	0	0	$\pi/2$	Global rotation (GR2)
6	$-\pi/2$	0	0	$-\pi/2$	Global rotation (GR3)

2.2 Equations of Motion

In this paper, the kinematics and dynamics of the human, robot, and table systems are studied using recursive kinematics and Lagrangian dynamics, and details refer to [6, 38]. The process is comprised of two parts: forward kinematics and backward dynamics. Forward kinematics transmits motion from the root to the end-effectors, while backward dynamics transfers forces from the end-effectors to the root. The system's dynamics equation can be written as [6, 38]

$$\tau_i = \mathrm{tr}\left(\frac{\partial \mathbf{A}_i}{\partial q_i}\mathbf{D}_i\right) - \mathbf{g}^{\mathrm{T}}\frac{\partial \mathbf{A}_i}{\partial q_i}\mathbf{E}_i - \mathbf{f}_k^{\mathrm{T}}\frac{\partial \mathbf{A}_i}{\partial q_i}\mathbf{F}_i - \mathbf{G}_i^{\mathrm{T}}\mathbf{A}_{i-1}\mathbf{z}_0 \quad (1)$$

where in the right side of Eq. (1), the first term is inertia and Coriolis torque, the second term is the torque due to gravity, the third term is the torque due to external forces, and the fourth term is the torque due to external moments. $\mathbf{A}_i$ is the global position transformation matrices (4×4) for the i^{th} joint.

$$\mathbf{D}_i = \mathbf{I}_i\mathbf{C}_i^{\mathrm{T}} + \mathbf{T}_{i+1}\mathbf{D}_{i+1} \quad (2)$$

$$\mathbf{E}_i = m_i\mathbf{r}_i + \mathbf{T}_{i+1}\mathbf{E}_{i+1} \quad (3)$$

$$\mathbf{F}_i = \mathbf{r}_k\delta_{ik} + \mathbf{T}_{i+1}\mathbf{F}_{i+1} \quad (4)$$

$$\mathbf{G}_i = \mathbf{h}_k\delta_{ik} + \mathbf{G}_{i+1} \quad (5)$$

In Eq. (1), $tr(\bullet)$ is the trace of a matrix, $\mathbf{C}_i$ is global acceleration transformation matrices, $\mathbf{I}_i$ is the inertia matrix for link i, $\mathbf{D}_i$ is the recursive inertia and Coriolis matrix, $\mathbf{E}_i$ is the recursive vector for gravity torque calculation, $\mathbf{F}_i$ is the recursive vector for external force-torque calculation, $\mathbf{G}_i$ is the recursive vector for external moment torque calculation, $\mathbf{g}$ is the gravity vector, m_i is the mass of link i, $\mathbf{r}_i$ is the center of mass (COM) of link i in the i^{th} local frame, $\mathbf{f}_k = [\ f_{kx}\ f_{ky}\ \ f_{kz}\ 0\ ]^{\mathrm{T}}$ is the external force applied on link k, $\mathbf{r}_k$ is the position of the external force in the k^{th} local frame, $\mathbf{h}_k = [\ h_x\ h_y\ \ h_z\ 0\ ]^{\mathrm{T}}$ is the external moment applied on link k, $\mathbf{z}_0 = [\ 0\ 0\ \ 1\ 0\ ]^{\mathrm{T}}$ is for a revolute joint, $\mathbf{z}_0 = [\ 0\ 0\ \ 0\ 0\ ]^{\mathrm{T}}$ is for a prismatic joint, finally, δ_{ik} is Kronecker delta, and the starting conditions are $\mathbf{D}_{n+1} = [\mathbf{0}]$ and $\mathbf{E}_{n+1} = \mathbf{F}_{n+1} = \mathbf{G}_{n+1} = [\mathbf{0}]$. The sensitivity to state variables is described in [6, 38].

2.2.1 Equation of Motion of Floating-base Table

The table only has six global DOFs (z_1, z_2, z_3, z_4, z_5, z_6) as shown in Fig. 1b, it is called a floating-base table. The grasping forces of the human and robot keep the table balanced with inertia and gravity forces during the lifting process, as shown below,

$$\tau_i = \mathrm{tr}\left(\frac{\partial \mathbf{A}_i}{\partial q_i}\mathbf{D}_i\right) - \mathbf{g}^{\mathrm{T}}\frac{\partial \mathbf{A}_i}{\partial q_i}\mathbf{E}_i - \mathbf{f}_k^{\mathrm{T}}\frac{\partial \mathbf{A}_i}{\partial q_i}\mathbf{F}_i = 0,\ \ i = 1,2,3,4,5,6 \quad (6)$$

where τ_i is the torque of the i^{th} virtual joint of the table. The virtual joint generates global motion for the table and has zero link mass except for the last joint as shown in Fig. 1b.

2.3 External Forces as Design Variables

External forces are expressed as fixed or variable components in Eq. (6). The grasping external forces between the human and the table are treated as design variables in this research. For this reason, the joint torques of the EOM are dependent on both state variables $\boldsymbol{q}$ and varying external forces (grasping forces). The sensitivity of joint torque to external force must be determined in order to perform gradient-based optimization. For example, for the single chain arm model, the external load in the vertical direction f_{ky} affects joint torques from the third term on the right hand side (RHS) of Eq. (6), the differentiation of τ_i with respect to f_{ky} can be calculated directly as:

$$\frac{\partial \tau_i}{\partial f_{ky}} = [\ 0\ 1\ \ 0\ 0\ ]\frac{\partial \mathbf{A}_i}{\partial q_i}\mathbf{F}_i \quad (7)$$

Furthermore, as illustrated in Fig. 2, the ground reaction force (GRF) is computed from human global joint torques. Considering the current state variables and external forces, joint torques can be calculated from the EOM without GRF. Then the resultant GRF can be obtained from the global joint torques at the point foot origin.

Similarly, the external loads f_{kx} and f_{kz} sensitivity can be computed as follows:

$$\frac{\partial \tau_i}{\partial f_{kx}} = [\,1\;0\;\;0\;0\,]\frac{\partial \mathbf{A}_i}{\partial q_i}\mathbf{F}_i \tag{8}$$

$$\frac{\partial \tau_i}{\partial f_{kz}} = [\,0\;0\;\;1\;0\,]\frac{\partial \mathbf{A}_i}{\partial q_i}\mathbf{F}_i \tag{9}$$

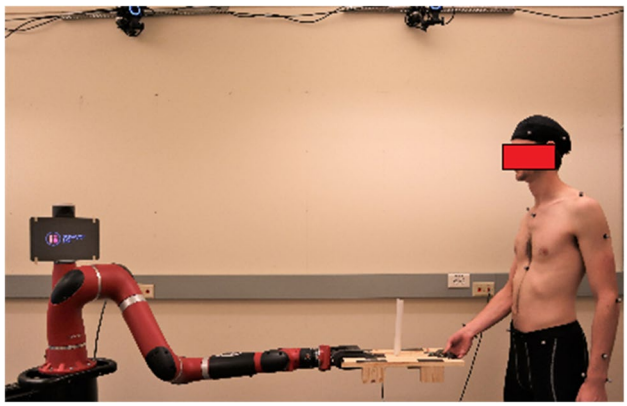

Fig. 3 Experiment for human–robot lifting

3 Human–robot Lifting Experiment

The Institutional Review Board (IRB) approved collaborative human–robot lifting study was conducted at Oklahoma State University with a single healthy male. Informed consent was obtained from the individual participant included in the study. OptiTrack motion capture (MOCAP) was used to obtain 3D kinematic data at 120 Hz. The room was surrounded by twelve prime 13W cameras. The subject was instructed to lift a 2 kg table with the robot collaboratively for the lifting task, as shown in Fig. 3. The data was processed using the motion capture software Motive 2.2 after the experiment. The data were smoothed and transformed into a C3D file after all markers were labeled. After that, the C3D file was imported into Visual 3D (C-Motion, Inc.). A skeletal model was constructed using the marker protocol used in the experiments, and it had a total of 9 segments. Coordinates, joint angles, and joint moments were generated using this skeleton model. The subject's anthropometric data were used to generate separate and accurate skeletal models, which enabled more precise calculations.

The positions at each robot joint from the simulation were provided in the robot operating system (ROS) to operate the robotic arm as shown in Fig. 4. The robot arm followed the optimal trajectory and executed the collaborative lifting task. We invoked the joint trajectory action server in velocity mode which allows trajectory execution by calculating and commanding the joint velocity required to move the arm through a set of joint positions at specified time instances [39]. The experiment was performed three times, and the robot's joint angle and joint torque profiles for each joint were collected. The collected data were postprocessed in MATLAB and compared the average of the three experimental trials against the predicted data.

The human hand grasping force was collected using force sensitive resistor (FSR) pads. These FSRs were attached to the lifting weight (table) (Fig. 5). This weight was a wooden board. There were four sensors on the bottom of the table and two on the top. A metal plate was attached to each set on the top and bottom to distribute the force evenly between FSRs. The subject grips the board using only one hand with his thumb contacting the top set of sensors, and his other four fingers contacting the bottom set of sensors. The resistance of each FSR was measured using a voltage divider circuit connected to an Arduino. The Arduino was controlled by a desktop computer running a MATLAB data acquisition system through a wired connection. The red arrows in Fig. 5 represent the location of the force vectors of the human's fingers.

A block diagram of the experimental table electronics is shown in Fig. 6. All six FSR pads were wired to an individual voltage divider circuits on a breadboard. The output signals of these voltage dividers were wired to the Arduino's analog input pins. The Arduino recorded a voltage reading from each voltage divider about every 0.3 s and transmitted

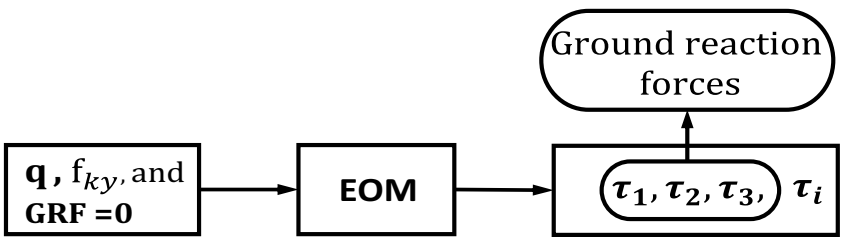

Fig. 2 Inverse dynamics calculation process

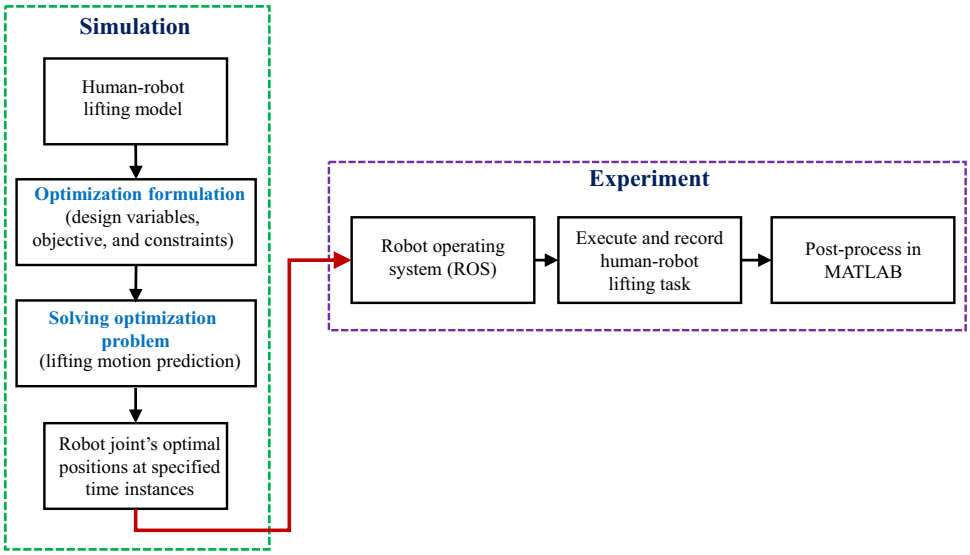

Fig. 4 Robot arm control strategy

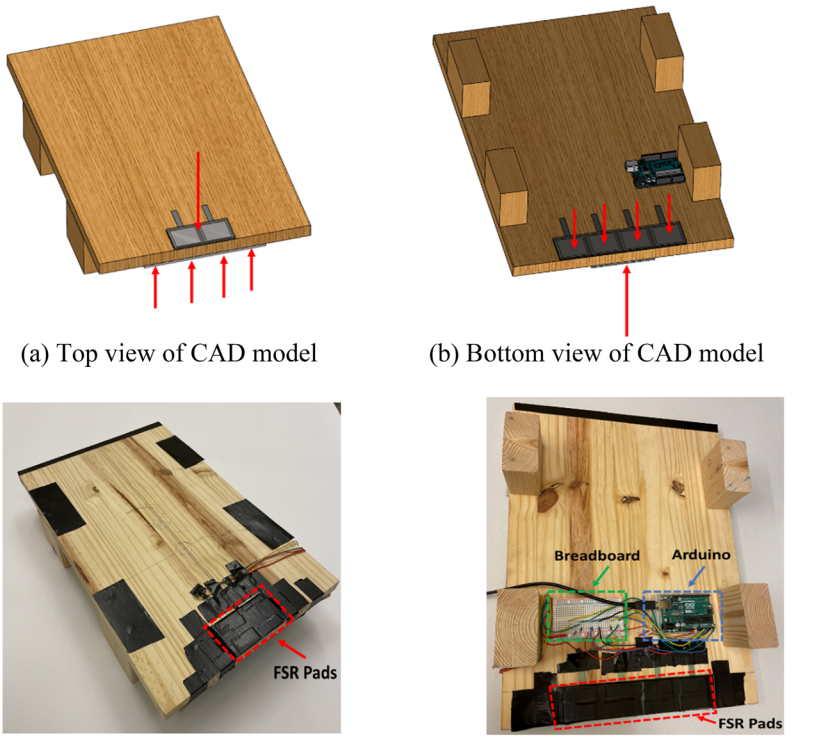

(a) Top view of CAD model (b) Bottom view of CAD model

(c) Top view of experimental table (d) Bottom view of experimental table

Fig. 5 Force sensors on lifting weight

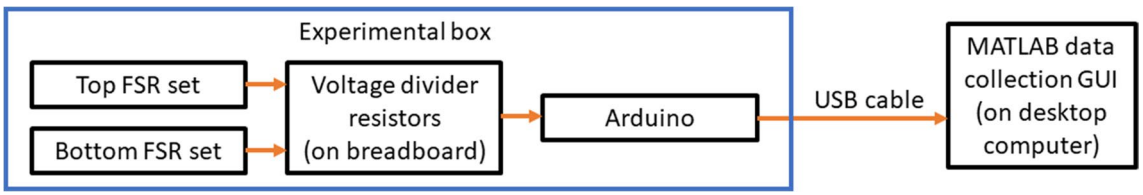

Fig. 6 Experimental force sensor data collection diagram

them to the MATLAB application on the desktop computer. The computer then used the calibration curve to calculate each sensor's force in grams.

The data collected by the Arduino was the output voltage (V_o) of a voltage divider circuit (Fig. 7a) for each sensor over time. This voltage divider is based on the recommendation of the FSR manufacturer. These sensors ideally have a one-to-one relationship between the applied load and the measured resistance. They do not have any dynamic effects. In order to determine the force corresponding to the detected voltages, the sensors were calibrated. A sensor was placed on a scale and incrementally loaded with 3-g weights. The voltage and scale weight values at each increment were recorded to produce a voltage vs force curve. This calibration process was performed four times, and a spline curve was fit to these four data sets (Fig. 7b). The spline served as a correlation between the recorded voltage and the actual force. Once the sensors were mounded on the experimental table with the metal plates taped against them, any preload on the sensors was subtracted out. To do this, the sensors were measured with no external force except for the weight of the metal plates and tension of the tape to determine if there was an unloaded non-zero force reading. This value for each sensor was subtracted from the recorded data to correct for preloading in the system.

A graphical user interface (GUI) was coded in MATLAB to start and stop the data recording and plot the sensor data as it was being collected (Fig. 8). After the experiment, the force from the top resistors was summed to get the force

Fig. 7 FSR setup and calibration

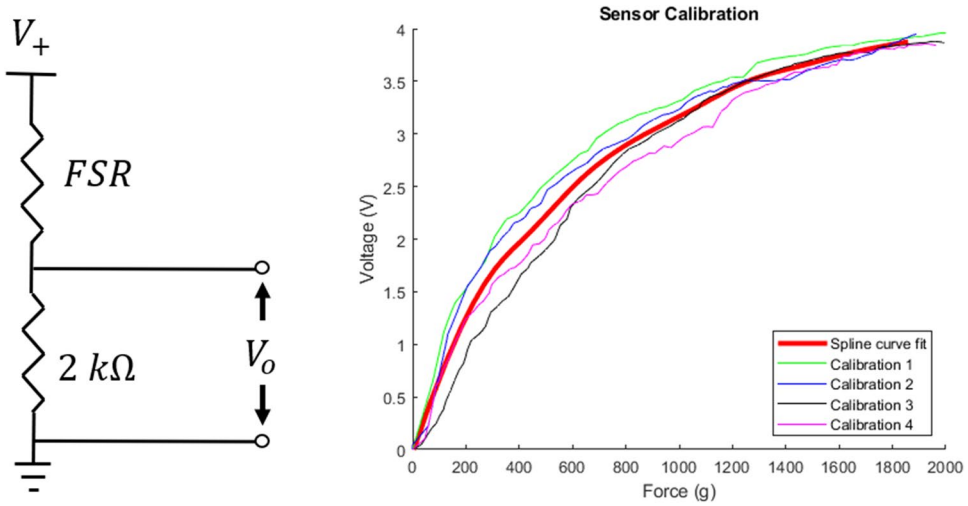

(a) Voltage divider circuit (b) Sensor calibration

Fig. 8 Data collection GUI

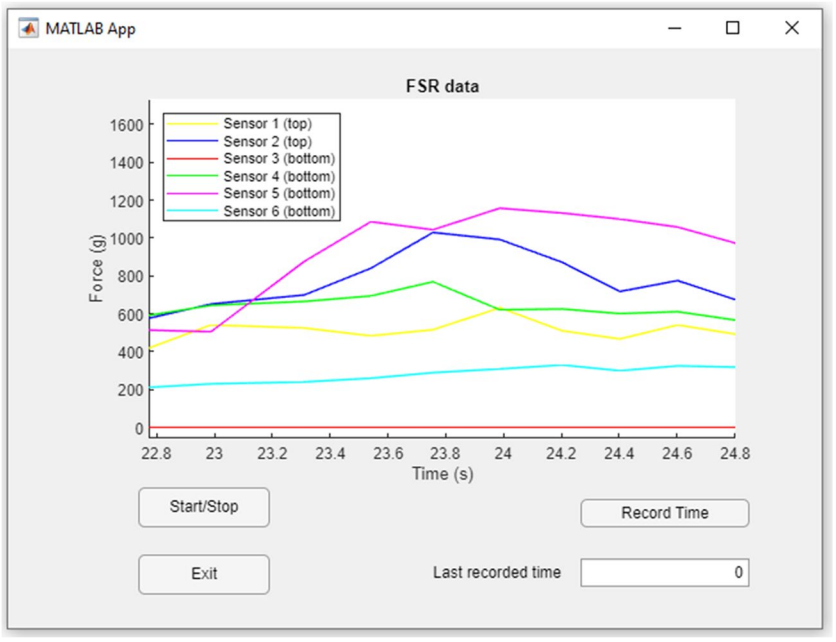

applied by the thumb, and the sum of the force of the bottom resistors determined the force applied by the four fingers. The four-finger force minus the thumb force determined the total experimental hand reaction (grasping) force.

4 Optimization Formulation

4.1 Design Variables

The design variables ($\mathbf{x}$) are joint angle control points $\mathbf{P}_{human}$, $\mathbf{P}_{robot,}$ and $\mathbf{P}_{table}$ for the human, robot, and table, since the joint angle profiles are discretized by cubic B-splines. Furthermore, the grasping forces ($\mathbf{f}_1^c$ and $\mathbf{f}_2^c$) between human and table, and robot and table, are treated as additional design variables. So, $\mathbf{x} = [\mathbf{P}_{human}^{\mathrm{T}}, \mathbf{P}_{robot}^{\mathrm{T}}, \mathbf{P}_{table}^{\mathrm{T}}, \mathbf{f}_1^{c\mathrm{T}}, \mathbf{f}_2^{c\mathrm{T}}]^{\mathrm{T}}$.

4.2 Objective Functions

The objective function is the sum of joint torques squared for human and robot [6, 40].

$$J(\mathbf{x}) = w_1 \sum_{i=3}^{n\_human} \int_0^T \{\tau_{i(human)}^2(\mathbf{P}_{human}, \mathbf{f}_1^c)\}dt + w_2 \sum_{i=3}^{n\_robot} \int_0^T \{\tau_{i(robot)}^2(\mathbf{P}_{robot}, \mathbf{f}_2^c)\}dt \tag{10}$$

where $n\_human = 13$, $n\_robot = 10$. The total time duration T is a specified input parameter, w_1 and w_2 are weighting coefficients for human and robot performance measure, respectively.

4.3 Constraints

The constraints presented in the following include (1) joint angle limits, (2) joint torque limits, (3) feet/robot base contacting position, (4) table forward position, (5) table range of motion, (6) table grasping location, and (7) table global EOM. Time independent constraints include (8) initial and final table locations and (9) static conditions at the beginning and end of the motion. For time-dependent constraints, constraints (1–4) are imposed for both the human and robotic arm, and constraints (5–7) are imposed for the table. Time-dependent constraints are calculated sequentially in the optimization process at every time discretization point. In contrast, the optimization calculates the time-independent constraints for the human and robotic arm at a specific time.

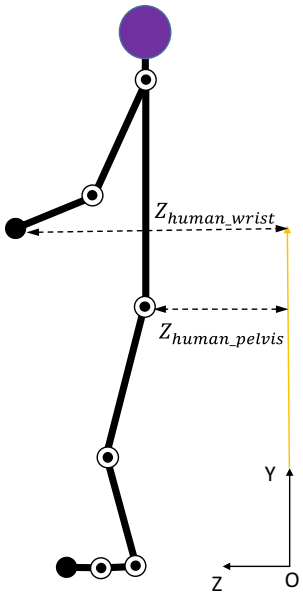

Fig. 9 Table forward position constraint

(1). Joint angle limits

$$\begin{aligned} \mathbf{q}_{human}^L \le \mathbf{q}_{human}(t) \le \mathbf{q}_{human}^U \\ \mathbf{q}_{robot}^L \le \mathbf{q}_{robot}(t) \le \mathbf{q}_{robot}^U \end{aligned} \tag{11}$$

where $\mathbf{q}_{human}^L$ and $\mathbf{q}_{robot}^L$ are the lower joint angle limits, and $\mathbf{q}_{human}^U$ and $\mathbf{q}_{robot}^U$ are the upper joint limits for the human and robot arm [41, 42], respectively.

(2). Joint torque limits

$$\begin{aligned} \boldsymbol{\tau}_{human}^L \le \boldsymbol{\tau}_{human}(t) \le \boldsymbol{\tau}_{human}^U \\ \boldsymbol{\tau}_{robot}^L \le \boldsymbol{\tau}_{robot}(t) \le \boldsymbol{\tau}_{robot}^U \end{aligned} \tag{12}$$

where $\boldsymbol{\tau}_{human}^L$ and $\boldsymbol{\tau}_{human}^U$ are human lower and upper joint torque limits, and $\boldsymbol{\tau}_{robot}^L$ and $\boldsymbol{\tau}_{robot}^U$ are robot lower and upper torque limits [41, 42], respectively.

(3). Point foot/robot base contacting position

$$\begin{aligned} p_{human\_foot}(t) = p_{human\_foot}^s \\ p_{robot\_base}(t) = p_{robot\_base}^s \end{aligned} \tag{13}$$

where $p_{human\_foot}(t)$ and $p_{robot\_base}(t)$ are calculated point human foot and robot base locations during the optimization process. $p_{human\_foot}^s$ and $p_{robot\_base}^s$ are the

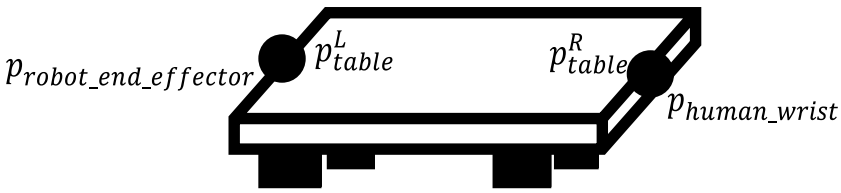

Fig. 10 Table grasping location constraint

specified point foot and robot base contacting positions on the level ground with fixed given values.

(4). Table forward position

$$Z_{human\_wrist}(t) - Z_{human\_pelvis}(t) \geq 0 \tag{14}$$

where Z_{human_wrist} and Z_{human_pelvis} are the global Z coordinates of wrist and pelvis points of the human, as shown in Fig. 9. This constraint ensures that the table remains in front of the human and prevents it from penetrating the human body.

(5). Table range of motion

$$\mathbf{q}^{L}_{table} \leq \mathbf{q}_{table}(t) \leq \mathbf{q}^{U}_{table} \tag{15}$$

where $\mathbf{q}^{L}_{table}$ is the lower table joint angle limits and $\mathbf{q}^{U}_{table}$ is the upper limit.

(6). Table grasping location

$$\begin{aligned} p_{human\_wrist}(t) - p^{R}_{table}(t) &= 0 \\ p_{robot\_end\_effector}(t) - p^{L}_{table}(t) &= 0 \end{aligned} \tag{16}$$

where p_{human_wrist} and $p_{robot\_end\_effector}$ are the wrist and end-effector (EE) positions of the human and robot arm, respectively. p^{L}_{table} and p^{R}_{table} are the left and right edge positions of the table as shown in Fig. 10.

(7). Table global EOM

$$\left|\tau^{table}_{i}\right| \leq \varepsilon, \; i = 1,2,3,4,5,6 \tag{17}$$

where $\boldsymbol{\tau}^{table}$ is the global joint force and torque values of the table, $\varepsilon = 1$N for force and $\varepsilon = 1$Nm for torque. To keep the table balanced, two external grasping forces act on the edges.

(8). Initial and final hand positions

$$\begin{aligned} p_{human\_hand}(t) &= p^{s}_{human\_hand}(t); t = 0, t = T \\ p_{robot\_EE}(t) &= p^{s}_{robot\_EE}(t) \end{aligned} \tag{18}$$

where $p_{human\_hand}(t)$ and $p_{robot\_EE}(t)$ are the calculated hand and robot end-effector (EE) positions in the optimization process. $p^{s}_{human\_hand}$ and $p^{s}_{robot\_EE}$ are the specified hand and EE positions at initial and final times.

(8). Initial and final static conditions

$$\begin{aligned} \ddot{\mathbf{q}}_{human}(t) &= \mathbf{0}; \; t = 0, \mathrm{t} = T \\ \ddot{\mathbf{q}}_{robot}(t) &= \mathbf{0} \\ \ddot{\mathbf{q}}_{box}(t) &= \mathbf{0} \end{aligned} \tag{19}$$

Table 5 Task parameters for the lifting

Parameters	
Table weight (kg)	2
Table width (m)	0.31
Table height (m)	0.02
Table depth (m)	0.45
Initial and final human feet contact position (m)	0.4
Vertical initial hand and EE position (m)	0.9
Initial and final robot base contact position (m)	0.85
Vertical final hand and EE position (m)	1.4
Standing distance, L(m)	1.9
T (s)	2.0

5 Numerical Results

The nonlinear programming problem (NLP) for human–robot lifting is solved using an SQP method in SNOPT [28]. The initial guess for the optimization is $\mathbf{P}^{T} = \left[\mathbf{P}^{T}_{human}, \mathbf{P}^{T}_{robot}, \mathbf{P}^{T}_{table}\right] = [\mathbf{0}]$, $\mathbf{f}^{c}_{1} = \mathbf{f}^{c}_{2} = [\mathbf{10}]$. There are a total of 224 design variables and 898 nonlinear constraints. The optimal solution was obtained in 15.93 s on a laptop with an Intel® Core™ i7 2.11 GHz CPU and 16 GB RAM. The input data related to the human–robot lifting task are given in Table 5.

First, Figs. 11 and 12 illustrate the snapshots of the predicted 3D human–robot arm lifting motion from the simulation and the experimental scenario. Figure 13 presents a comparison of experimental and simulation joint angles for human shoulder flexion and elbow flexion. Furthermore, the joint torque profiles for human shoulder flexion, and elbow flexion are shown in Fig. 14. Human table grasping force comparisons are presented in Fig. 15. Figure 16 shows the comparison of experimental and simulation joint angle profiles for the robot arm. The experimental trials for robot joint torque

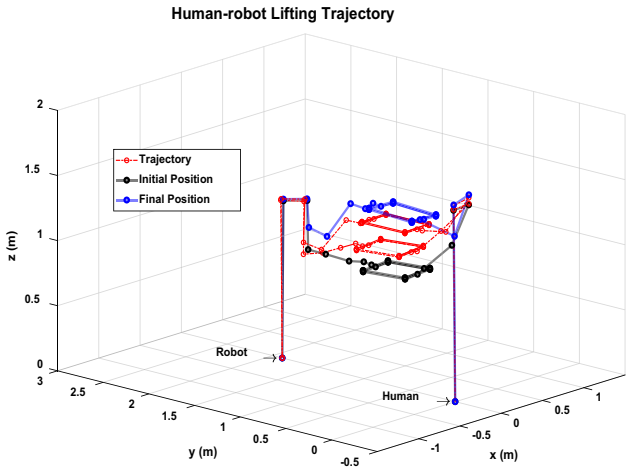

Fig. 11 Simulation snapshots for human–robot lifting

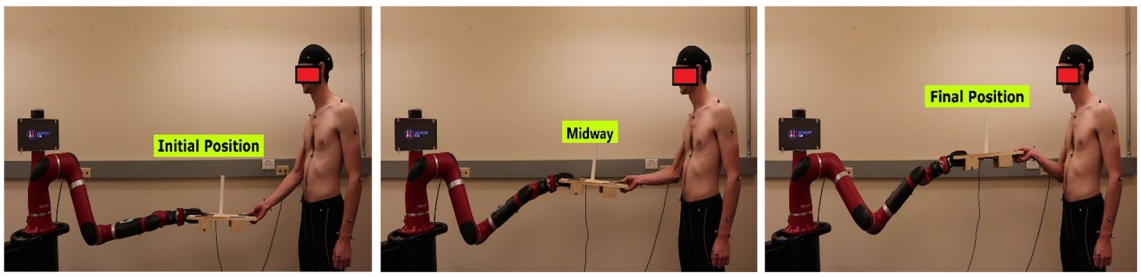

Fig. 12 Experiment snapshots for human–robot lifting

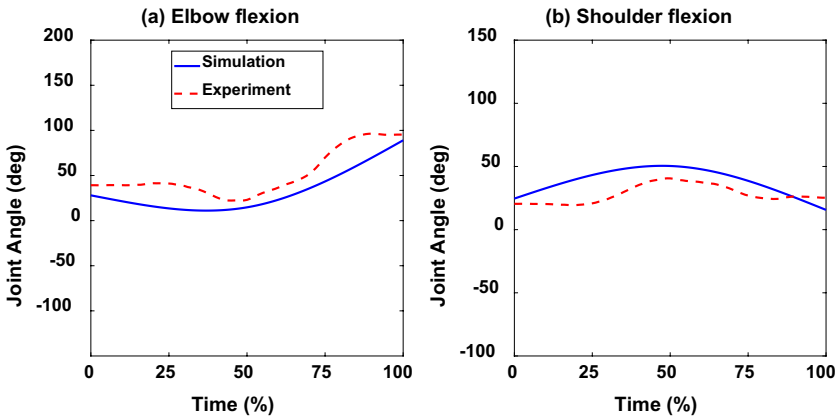

Fig. 13 Human arm joint angle profiles comparison between simulation and experiment

trajectories are shown in Fig. 17. Finally, Fig. 18 provides the comparison of experimental and simulation joint torque profiles for the robot arm.

6 Discussion and Conclusions

The trajectory of the simulated human–robot lifting motion and the human–robot initial, midway, and final position in the experiment are depicted in Figs. 11 and 12. In this study, the optimization predicts a natural collaborative lifting motion. In Fig. 13, the trends of the predicted human joint angle profiles closely follow the experimental joint angle profiles. However, the predicted elbow flexion values are less than the experimental elbow flexion values, and the peak values difference between them is 10.69%. For the shoulder flexion joint angle profiles, predicted values are higher than the experimental values until 90% of the lifting cycle, and the peak values difference between the prediction and experiment is 19.56%. These deviations

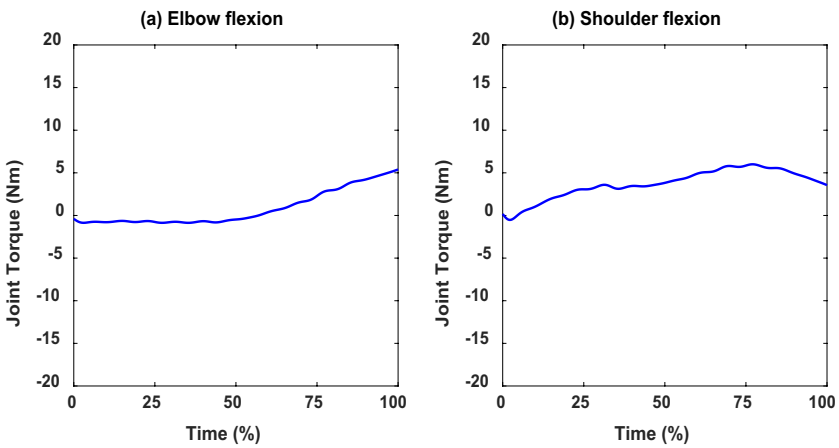

Fig. 14 Human arm joint torque profiles

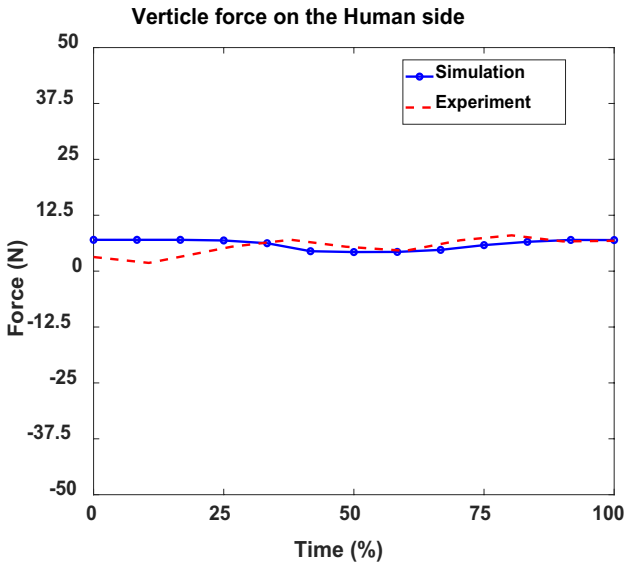

Fig. 15 Human table grasping force comparison between simulation and experiment

may be due to lack of constraints on the subject's arm motion in the experiment. In addition, the lifting trajectory may differ from subject to subject, and it is quite difficult to follow the simulation results precisely in a real-world scenario. Furthermore, when the joint angle increases, as shown in Fig. 13, so does the magnitude of the simulated joint torque profile of elbow flexion (Fig. 14). In the same way, the magnitude of the joint torque profile of the shoulder flexion follows the joint angle trends, as illustrated in Fig. 14.

In the comparison of human table grasping forces shown in Fig. 15, the experimental vertical grasping force on the human side is initially lower than the simulated force. The experimental force, however, follows the simulated grasping force after the first 25% of the overall lifting duration. Five force sensors were utilized in the experiment, and it is anticipated that naturally, the human did not press the sensors adequately at first. Overall, the predicted vertical grasping force values closely follow the trends of the experimental data. The peak value difference between the predicted and the experimental vertical grasping forces is 12.52%.

The joint angles of the robot arm in the simulation and experiment are identical, as shown in Fig. 16. The positions at each joint are provided from the simulation. The magnitudes and the trends of the robot joint torques for three experimental trials are similar as shown in Fig. 17. Moreover, the average of three trials is taken to compare against the predicted robot joint torques. The joint torques of the robot arm are compared in Fig. 18, and the predicted robot joint torques have similar trends to experimental robot joint torques. The robot's third joint has the largest peak value difference of 18.03%, and the second joint has the lowest peak value difference of 3.72%, between the predicted and experimental data.

Fig. 16 Robot arm joint angles comparison between simulation and experiment

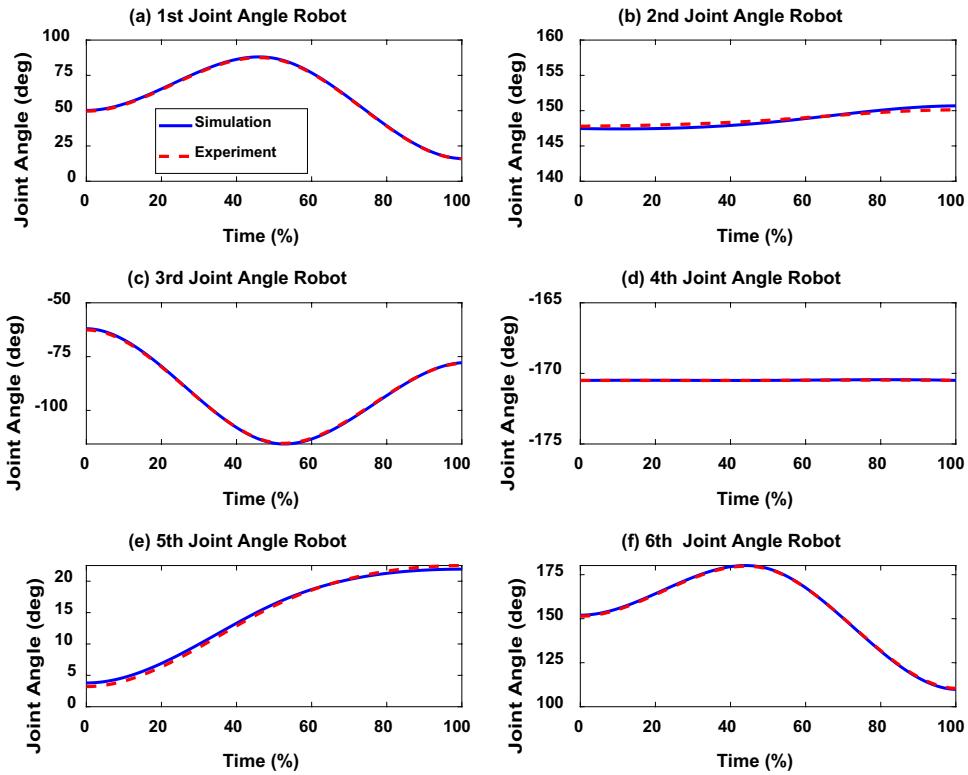

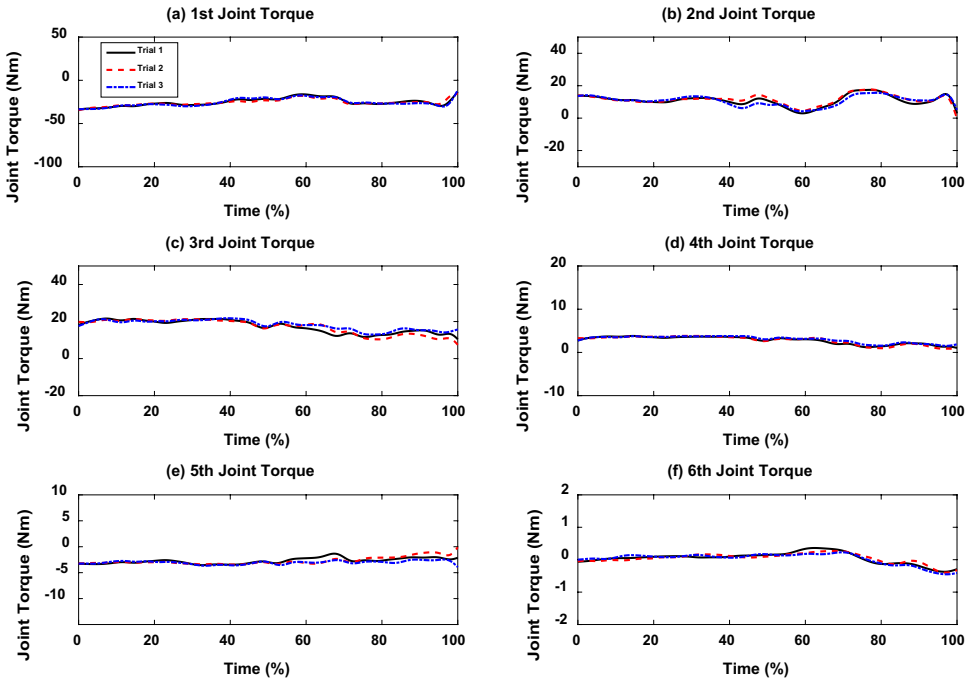

Fig. 17 Robot arm joint torque trajectories for three experimental trials

In this study, an inverse dynamics optimization formulation was used to predict human–robot lifting motion and grasping forces. The NLP optimization problems were successfully solved by SNOPT, a gradient-based optimizer. The simulation results were compared to the experimental data, including human joint angle profiles from motion capture, robot joint torque profiles, and hand grasping force profiles from force sensors. The proposed optimization formulation can be used to design the best human–robot collaborative lifting to prevent human injury.

In addition, the human–robot collaborative lifting was carried out without using any learning techniques. The

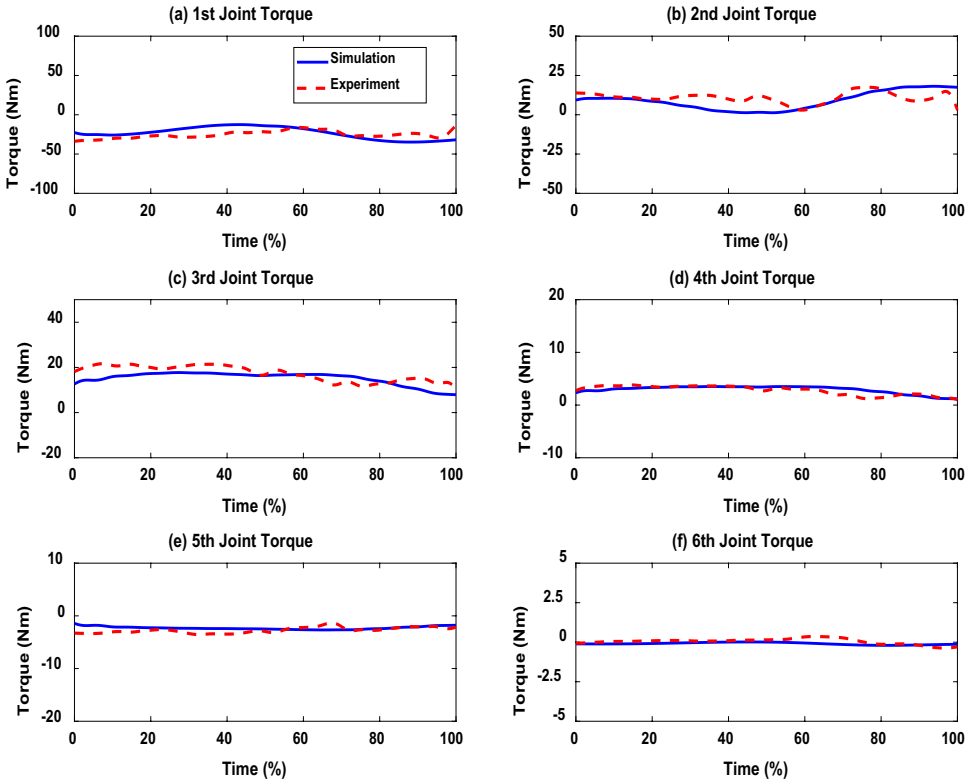

Fig. 18 Robot arm joint torques comparison between simulation and experiment

simulation provided the robot's position, velocity, and acceleration at each joint, and the human adapted to the robot during the lifting. The next goal is to establish a lifting database, and we will conduct the experiments and simulations with different subjects and varying table weights [33] in the future. In addition, a 3D musculoskeletal model will be considered to simulate human–robot collaborative lifting motion.

Acknowledgements This study is partially supported by Grant No. T42OH008421 from the National Institute for Occupational Safety & Health (NIOSH) to the Southwest Center for Occupational and Environmental Health (SWCOEH), National Science Foundation project 1849279 and 2014281, and Research Jumpstart/Accelerator Grant from Oklahoma State University. We thank anonymous reviewers for providing us the valuable suggestions to improve the presentation of the material in this study.

Authors' Contributions Conceptualization, Y.X.; methodology, A.A. and Y.X.; validation, A.A., J.Q. and S.S.; formal analysis, A.A., J.Q. and S.S.; data curation, A.A., J.Q. and S.S.; writing—original draft preparation, A.A., J.Q., and Y.X.; writing—review and editing, Y.X. and H.B.; supervision, Y.X. and H.B.; project administration, Y.X.; funding acquisition, Y.X. All authors have read and agreed to the published version of the manuscript.

Funding This work was supported by Grant No. T42OH008421 from the National Institute for Occupational Safety & Health (NIOSH/CDC) to the Southwest Center for Occupational and Environmental Health (SWCOEH), National Science Foundation project CBET 1849279 and 2014281, and Research Jumpstart/Accelerator Grant from Oklahoma State University. All these grants are funded to Y.X.

Data Availability No.

Code Availability No.

Declarations

Ethics Approval The human subject experiment was approved by Institutional Review Board at Oklahoma State University. The IRB number is IRB-21–501.

Consent to Participate Informed consent was obtained from all individual participants included in the study.

Consent for Publication The authors affirm that human research participants provided informed consent for publication of the images in Figure(s) 3 and 12.

Conflicts of Interest The authors declare they have no financial interests.

References

1. Bauer, A., Wollherr, D., Buss, M.: Human–robot collaboration: a survey. Int. J. Humanoid Rob. **5**(01), 47–66 (2008)
2. Rozo, L., Calinon, S., Caldwell, D.G., Jimenez, P., Torras, C.: Learning physical collaborative robot behaviors from human demonstrations. IEEE Trans. Rob. **32**(3), 513–527 (2016)
3. Xiang, Y., Arora, J.S., Rahmatalla, S., Marler, T., Bhatt, R., Abdel-Malek, K.: Human lifting simulation using a multi-objective optimization approach. Multibody Sys.Dyn. **23**(4), 431–451 (2010)
4. Xiang, Y., Arora, J.S., Abdel-Malek, K.: 3D human lifting motion prediction with different performance measures. Int. J. Humanoid Rob. **9**(02), 1250012 (2012)
5. Song, J., Qu, X., Chen, C.H.: Simulation of lifting motions using a novel multi-objective optimization approach. Int. J. Ind. Ergon. **53**, 37–47 (2016)
6. Xiang, Y., Arefeen, A.: Two-dimensional team lifting prediction with floating-base box dynamics and grasping force coupling. Multibody Sys.Dyn. **50**, 211–231 (2020)
7. Wang, Q., Xiang, Y., Kim, H.J., Arora, J.S., Abdel-Malek, K.: Alternative formulations for optimization-based digital human motion prediction. Proceedings of 2005 Digital Human Modeling for Design and Engineering Symposium, June 14–16, Iowa City, IA, SAE Technical Paper 2005–01–2691. (2005)
8. Evrard, P., Gribovskaya, E., Calinon, S., Billard, A., and Kheddar, A.: Teaching physical collaborative tasks: object-lifting case study with a humanoid. 2009 9th IEEE-RAS International Conference on Humanoid Robots, December 7–10, Paris, France, pp. 399–404. (2009)
9. Evrard, P., Kheddar, A.: Homotopy switching model for dyad haptic interaction in physical collaborative tasks. In World Haptics Third Joint EuroHaptics Conference and Symposium on Haptic Interfaces for Virtual Environment and Teleoperator Systems (pp. 45-50). IEEE, Salt Lake City, UT, USA (2009)
10. DelPreto, J., Rus, D.: Sharing the load: human-robot team lifting using muscle activity, in 2019 IEEE International Conference on Robotics and Automation (ICRA), May 20–24, Montreal, Canada. (2019)
11. Calinon, S., Evrard, P., Gribovskaya, E., Billard, A. and Kheddar, A.: Learning collaborative manipulation tasks by demonstration using a haptic interface. In: 2009 International Conference on Advanced Robotics, pp.1–6, June 22–26, Munich, Germany. (2009)
12. Agravante, D.J., Cherubini, A., Bussy, A., Gergondet, P., Kheddar, A.: Collaborative human-humanoid carrying using vision and haptic sensing. In 2014 IEEE International Conference on Robotics and Automation (ICRA) (pp. 607–612). IEEE, Hong Kong, China (2014)
13. Lawitzky, M., Medina, J.R., Lee, D., Hirche, S.: Feedback motion planning and learning from demonstration in physical robotic assistance: differences and synergies. In 2012 IEEE/RSJ International Conference on Intelligent Robots and Systems (pp. 3646–3652). IEEE, Vilamoura-Algarve, Portugal (2012)
14. Sheng, W., Thobbi, A., Gu, Y.: An integrated framework for human–robot collaborative manipulation. IEEE Trans. Cybern. **45**(10), 2030–2041 (2014)
15. Rozo, L., Calinon, S., Caldwell, D., Jiménez, P., Torras, C.: Learning collaborative impedance-based robot behaviors. In Proceedings of the AAAI Conference on Artificial Intelligence (Vol. 27, No. 1, pp. 1422–1428). Bellevue, Washington USA (2013)
16. Rozo, L., Bruno, D., Calinon, S. and Caldwell, D.G.: Learning optimal controllers in human-robot cooperative transportation tasks with position and force constraints. In 2015 IEEE/RSJ International Conference on Intelligent Robots and Systems (IROS) (pp. 1024–1030). September 28-October 2, Hamburg, Germany. IEEE. (2015)
17. Wang, Z., Peer, A. and Buss, M.: An HMM approach to realistic haptic human-robot interaction. In World Haptics 2009-Third Joint EuroHaptics Conference and Symposium on Haptic Interfaces for Virtual Environment and Teleoperator Systems (pp. 374–379). March 18–20, Salt Lake City, UT, USA. IEEE. (2009)
18. Mörtl, A., Lawitzky, M., Kucukyilmaz, A., Sezgin, M., Basdogan, C., Hirche, S.: The role of roles: Physical cooperation between

humans and robots. The Int. J. Robot. Res. **31**(13), 1656–1674 (2012)
19. Bussy, A., Gergondet, P., Kheddar, A., Keith, F., Crosnier, A.: Proactive behavior of a humanoid robot in a haptic transportation task with a human partner. In 2012 IEEE RO-MAN: The 21st IEEE International Symposium on Robot and Human Interactive Communication (pp. 962–967). IEEE, Paris, France (2012)
20. Li, Y., Ge, S.S.: Human–robot collaboration based on motion intention estimation. IEEE/ASME Trans. Mechatron. **19**(3), 1007–1014 (2013)
21. Passenberg, C., Groten, R., Peer, A., Buss, M.: Towards real-time haptic assistance adaptation optimizing task performance and human effort. In 2011 IEEE World Haptics Conference (pp. 155–160). IEEE, Istanbul, Turkey (2011)
22. Peternel, L., Kim, W., Babič, J., Ajoudani, A.: Towards ergonomic control of human-robot co-manipulation and handover. In 2017 IEEE-RAS 17th International Conference on Humanoid Robotics (Humanoids) (pp. 55–60) November 15–17. IEEE, Birmingham, UK (2017)
23. van der Spaa, L., Gienger, M., Bates, T. and Kober, J.: Predicting and optimizing ergonomics in physical human-robot cooperation tasks. In 2020 IEEE International Conference on Robotics and Automation (ICRA) (pp. 1799–1805). May 31-August 31, virtual conference. IEEE. (2020)
24. Arefeen, A., Xiang, Y.: Design human-robot collaborative lifting task using optimization. Proceedings of the ASME 2021 International Design Engineering Technical Conferences and Computers and Information in Engineering Conference. Volume 2: 41st Computers and Information in Engineering Conference (CIE). August 17–19, 2021, Online, V002T02A010. (2021)
25. Wojtara, T., Uchihara, M., Murayama, H., Shimoda, S., Sakai, S., Fujimoto, H., Kimura, H.: Human–robot collaboration in precise positioning of a three-dimensional object. Automatica **45**(2), 333–342 (2009)
26. Maurice, P., Huber, M.E., Hogan, N., Sternad, D.: Velocity-curvature patterns limit human–robot physical interaction. IEEE Robot. Autom. Lett. **3**(1), 249–256 (2017)
27. Parker, C.A., Croft, E.A.: Experimental investigation of human-robot cooperative carrying. In 2011 IEEE/RSJ International Conference on Intelligent Robots and Systems (pp. 3361–3366). September 25–30. IEEE, San Francisco, CA, USA (2011)
28. Gill, P.E., Murray, W., Saunders, M.A.: SNOPT: An SQP algorithm for large-scale constrained optimization. SIAM J. Optim. **12**(4), 979–1006 (2002)
29. Lorenzini, M., Kim, W., De Momi, E., Ajoudani, A.: A synergistic approach to the real-time estimation of the feet ground reaction forces and centers of pressure in humans with application to human–robot collaboration. IEEE Robot. Autom. Lett. **3**(4), 3654–3661 (2018)
30. Roveda, L., Haghshenas, S., Caimmi, M., Pedrocchi, N., Molinari Tosatti, L.: Assisting operators in heavy industrial tasks: On the design of an optimized cooperative impedance fuzzy-controller with embedded safety rules. Front. Robot. AI **6**, 75 (2019)
31. Kim, W., Lee, J., Peternel, L., Tsagarakis, N., Ajoudani, A.: Anticipatory robot assistance for the prevention of human static joint overloading in human–robot collaboration. IEEE Robot. Autom. Lett. **3**(1), 68–75 (2017)
32. Sartore, C., Rapetti, L., Pucci, D.: Optimization of humanoid robot designs for human-robot ergonomic payload lifting. In 2022 IEEE-RAS 21st International Conference on Humanoid Robots (Humanoids) (pp. 722–729). November 28–30. IEEE, Ginowan, Japan (2022)
33. Al-Yacoub, A., Zhao, Y.C., Eaton, W., Goh, Y.M., Lohse, N.: Improving human robot collaboration through Force/Torque based learning for object manipulation. Robot. Comput. Integr. Manuf. **69**, 102111 (2021)
34. Arefeen, A., Xiang, Y.: Modeling and simulation of a powered exoskeleton system to aid human-robot collaborative lifting. In Proceedings of the 7th International Digital Human Modeling Symposium (DHM 2022) and Iowa Virtual Human Summit 2022 (Vol. 7, No. 1), August 29–31, Iowa city, IA, USA. (2022)
35. Denavit, J., Hartenberg, R.S.: A kinematic notation for lower-pair mechanisms based on matrices. J. Appl. Mech. **22**, 215–221 (1955)
36. Cheng, H., Obergefell, L., and Rizer, A.: Generator of body (GEBOD) manual, AL/CF-TR-1, Dayton, OH, USA. (1994)
37. Wang Y., Kong X., Yang J., Zhao G.: Motion performance analysis of the sawyer ankle rehabilitation robot. In: Tan J. (eds) Advances in Mechanical Design. ICMD 2019. Mechanisms and Machine Science, vol 77. Springer, Singapore.994–0051, Armstrong Laboratory, Wright-Patterson Air Force Base, Ohio. (2020)
38. Xiang, Y., Arora, J.S., Rahmatalla, S., Abdel-Malek, K.: Optimization-based dynamic human walking prediction: one step formulation. Int. J. Numer. Meth. Eng. **79**(6), 667–695 (2009)
39. Rethink robotics, 2022, Arm control system. Retrieved on February 10, 2022 from https://support.rethinkrobotics.com/support/solutions/articles/80000980284-arm-control-system#Joint-Control-Modes
40. Arefeen, A., Xiang, Y.: Two-dimensional team lifting prediction with different box weights. Proceedings of the ASME 2020 International Design Engineering Technical Conferences and Computers and Information in Engineering Conference. Volume 9: 40th Computers and Information in Engineering Conference (CIE). August 17–19, 2020, Online, V009T09A004. (2020)
41. Xiang, Y., Zaman, R., Rakshit, R., Yang, J.: Subject-specific strength percentile determination for two-dimensional symmetric lifting considering dynamic joint strength. Multibody Sys.Dyn. **46**(1), 63–76 (2019)
42. Xiang, Y., Cruz, J., Zaman, R., Yang, J.: Multi-objective optimization for two-dimensional maximum weight lifting prediction considering dynamic strength. Eng. Optim. **53**(2), 206–220 (2021)

Asif Arefeen received the bachelor's degree in Aeronautical Engineering from the Military Institute of Science and Technology, Bangladesh, in 2014, and Master and Ph.D. degrees from Oklahoma State University, Stillwater, OK, USA, in 2019 and 2023, respectively. He is currently a postdoctoral scholar in the School of Medicine, Biomedical Engineering Department at Case Western Reserve University, Cleveland, OH, USA. His research interests include human-robot interaction, wearable robotics, biomechanics, optimal control, and gradient-based optimization.

Joel Quarnstrom is a Mechanical and Aerospace Engineering PhD student studying robotics and controls at Oklahoma State University (OSU). He graduated with his B.S. in Mechanical Engineering with a second major in Physics in the Spring of 2022. He works in the Biodynamics Optimization and Motion Control Lab at OSU. In this lab he has conducted research on a novel arm rehabilitation device, human-robot interaction biomechanics study, and a bio-inspired inchworm robot. He also collaborated with an Electrical Engineering Lab at OSU on a home care robot intended to benefit the elderly.

Shahbaz P Qadri Syed is currently pursuing his PhD in Mechanical and Aerospace Engineering at Oklahoma State University, Stillwater, OK, USA. Prior to this, he received his M.S degree in Mechanical and Aerospace Engineering from Oklahoma State University in 2022, and his B.E degree in Mechanical Engineering from Osmania University, Hyderabad, India in 2019. His research interests include control theory, machine/reinforcement learning, probabilistic inference, and their intersections applied to multiagent systems.

He Bai received his B.S. degree from the Department of Automation at the University of Science and Technology of China, Hefei, China, in 2005, and the M.S. and Ph.D. degrees in Electrical Engineering from Rensselaer Polytechnic Institute in 2007 and 2009, respectively. From 2009 to 2010, he was a Post-doctoral Researcher at Northwestern University, Evanston, IL. From 2010 to 2015, he was a Senior Research and Development Scientist at UtopiaCompression Corporation. In 2015, he joined the Mechanical and Aerospace Engineering Department at Oklahoma State University, where he is currently an associate professor. His research interests include multi-agent learning and control, nonlinear estimation, robotics, and autonomous systems.

Yujiang (Mike) Xiang is currently an Associate Professor in the Department of Mechanical and Aerospace Engineering at Oklahoma State University (OSU). He received his B.S. and M.S. degrees in Automotive Engineering from Tsinghua University in 2001 and 2004, respectively, and Ph.D. degree from the University of Iowa in 2008. He directs Biodynamics Optimization and Motion Control Lab in OSU. His current research interests include human robot interaction, musculoskeletal modeling, motion biomechanics, assistive robots, and exoskeletons.